ELSEVIER

Quasi-Instantaneous and Long-Term Deformations of High Performance Concrete with Sealed Curing

Bertil Persson
Division of Building Materials, Lund Institute of Technology, Lund, Sweden

This article outlines an experimental and numerical study on quasi-instantaneous and long-term deformations of high performance concrete subjected to sealed curing. For this purpose more than 100 cylinders and 400 cubes were made of eight concretes and studied in relation to creep and shrinkage, hydration, internal relative humidity, and compressive strength. One heat-cured concrete was studied at temperatures other than 20°C varying between −20°C and 60°C. Analyses were carried out of quasi-instantaneous deformation, short- and long-term basic creep, and autogenous shrinkage. Relationships were obtained between elastic modulus and creep compliance, and hydration, internal relative humidity, and compressive strength. New and original results are presented on relationships between autogenous shrinkage and internal relative humidity. Other results confirm and validate earlier findings of normal strength concrete regarding relationships between creep compliance, porosity, compressive strength, and maturity for high performance concrete. The project was carried out at Lund Institute of Technology between 1992 and 1996. Advanced Cement Based Materials 1998, 8, 1–16. © *1998 Elsevier Science Ltd.*
KEY WORDS: Basic creep, Compressive strength, Creep compliance, High performance concrete, Internal relative humidity, Maturity, Porosity, Self-desiccation, Silica fume

High strength, increased durability, and self-desiccation characterize high performance concrete (HPC). Use of low alkaline cement, low water/cement ratio (w/c), high quality aggregate, and addition of silica fume and superplasticizer provided those properties. Aggregate grading was chosen in a semi-logarithmic way [1] and the concrete mixing was performed in a special order, i.e., the superplasticizer was added at the end of the mixing. It was possible to mix, transport, pump, and pour HPC in the same manner as normal strength concrete (NSC). Until now HPC has been used mainly in high rise buildings, bridges, and oil platforms [2]. A special application called self-desiccating slabs was used for more than 1 million m^2 of floors of dwelling houses in Sweden [3] and Finland [4]. However, more general use of HPC necessitates more research on the long-term properties of HPC, especially at early ages [5].

Address correspondence to: Mr. Bertil Persson, Division of Building Materials, Lund Institute of Technology, Box 118, S-221 00 Lund, Sweden.
Received October 27, 1997; Accepted December 10, 1997.

Objectives

The main objective of the study was to investigate elastic and long-term deformations of HPC subjected to sealed curing (with some related properties) at early ages by observing deformations of young HPC subjected to sustained loading in a constant environment. Mature HPC was studied as a reference. Studies at various temperatures other than 20°C were carried out on one HPC in order to determine the effect of heat curing. Parameters such as compressive strength, hydration, and self-desiccation were studied parallel to creep. Effects of aggregate, w/c, type and amount of silica fume, and air-entraining on creep were investigated.

Materials and Experimental Methods

Materials

Table 1 shows the properties of the aggregates and silica fumes used in the experiments [6,7]. The composition of the low alkaline cement used is shown in Table 2 [7]. The air-entraining agent was of type vinsole resin. The superplasticizer was based on melamine formaldehyde. Table 3 provides the mix composition and the principal properties of the concretes studied [7].

Specimens

Cylinders 300 mm long and 55 mm in diameter were used to perform the creep studies. At the start of the investigation the minimum specified specimen size was 3 times the maximum size of the aggregate. The specimens were actually made with a diameter of 3.6 times the aggregate size. However, after the experiments began, new guidelines were introduced suggesting a

ISSN 1065-7355/98/$19.00
PII S1065-7355(98)00004-2

TABLE 1. Properties of the aggregates and the silica fume used in the experiments [6,7]

Properties	Elastic Modulus (GPa)	Compressive Strength (MPa)	Split Tensile Strength (MPa)	Ignition Losses (%)	Fineness (m^2/g)
Crushed sand	59.1	234	14.3	1.95	
Granite	61.2	153	9.6	1.67	
Natural sand/pea gravel				0.79/1.62	
Quartzite sandstone	60.2	332	15.0	0.28	
Granulated silica fume				2.26	17.5
Silica fume slurry				1.86	22.5

TABLE 2. Composition of cement [7]

Component	(%)
Analyzed properties	
CaO	64.6
SiO_2	21.8
Al_2O_3	3.34
Fe_2O_3	4.39
MgO	0.84
K_2O	0.62
Na_2O	0.07
Alkali	0.48
SO_3	2.23
CO_2	0.14
Ignition losses	0.63
Free CaO	1.13
Mineralogical properties	
C_2S	22.5
C_3S	53.0
C_3A	1.42
C_4AF	13.4
Physical properties	
Blaine fineness	325 m^2/kg
Density	3180 kg/m^3

minimum specimen size of 5 times the maximum aggregate [8]. No evidence was found to corroborate that the so-called skin effect of the specimen would affect the measured creep on seal-cured specimens with cross-section diameter of 3.6 times the maximum aggregate instead of 5 times [9]. The size of the specimen was chosen to avoid temperature effects on the deformations at early ages. Hydration, self-desiccation and compressive strength were studied on 100-mm cubes that were made from the same batch of HPC. Compressive strength tests also were conducted on cylinders of the same size as those used in the creep tests. Table 4 shows a summary of numbers of specimens used in the experiments [7].

Mixing and casting of the concretes took place according to the following steps [7]:

1. The moisture of the gravel was adjusted to about 4%. The amount of moisture was accounted for in the calculations of w/c.

TABLE 3. Composition (kg/m^3 dry material) and properties of the concretes [7]

Concrete	1	2	3	4	5	6	7	8
Quartzite sandstone 8–12 mm	460							
Quartzite sandstone 12–16 mm	460	965	930		1020	1005		1060
Natural sand A 0–8 mm	810	850	790		765	765		750
Granite 12–16 mm, N							1065	
Pea gravel 8–16 mm				1075				
Natural sand 0–8 mm				780			770	
Cement	430	445	450	450	500	525	480	540
Granulated silica fume	22	45	45		50	53		54
Silica fume slurry				23			48	
Air-entraining agent	0.02		0.04					
Superplasticizer	2.8	5.5	4.3	5.3	4.8	6.4	7.8	9.6
Water-cement ratio (w/c)	0.375	0.37	0.365	0.33	0.31	0.30	0.30	0.25
Air content (% by total volume)	4.0	0.9	4.5	0.9	0.9	0.9	0.9	1.0
Density (kg/m^3)	2330	2475	2380	2480	2500	2510	2520	2540
Aggregate content	0.742	0.733	0.723	0.748	0.714	0.705	0.728	0.713
Slump (mm)	140	160	170	145	200	230	45	45
28-day compressive strength (MPa)	89	110	92	101	127	137	122	143
1-year compressive strength (MPa)	101	124	108	115	139	144	135	162
2-year compressive strength (MPa)	112	127	121	115	145	149	131	162
4-year compressive strength (MPa)	102	135	109	113	141	139	129	162

TABLE 4. Numbers of specimens [7]

Parameter	Cylinders	Cubes
Short-term creep	37	
Long-term creep	33	
Autogenous shrinkage	33	
Compressive strength	32	400
Internal relative humidity		400
Hydration		400

2. Materials except water, air-entraining agent, and superplasticizer were mixed for ½ minute.
3. Water and air-entraining agent were added to the mix and mixed for another ½ minute.
4. Finally, the superplasticizer was added to the mix and mixed for another 3 minutes.
5. The concrete was cast in steel molds (cylinders or cubes) and vibrated for ½ minute.
6. The specimens were sealed-cured at constant temperature 20°C (the maximum rise of temperature of the concrete internally was 4°C).
7. After 16 hours the specimens were demolded and sealed with 2-mm vulcanized butyl rubber.
8. Steel items cast in the concrete were connected to the measurement devices items on three sides of the specimen by steel bolts through the sealing of butyl rubber.
9. Initial measurements were taken within 1 hour after demolding.

Experimental Methods

The short-term studies were performed in an MTS machine, from 0.01 seconds of loading until 66 hours. Parallel studies of basic creep were carried out in traditional spring-loading devices [7], from 1 minute of loading until about 2 years. Autogenous shrinkage was studied at the same loading time as the creep and in the same environment. Fragments of the cubes that were used to obtain the compressive strength were also used to obtain the internal relative humidity and the degree of hydration [10]. The same batch of concrete was used for each experiment type. The stress to cube compressive strength ratio was either 0.3 or 0.6. The stress to cylinder compressive strength ratio was calculated as 0.43 and 0.86, respectively, at start of the testing [11]. The age of the concrete was either 1 or 2 days at loading of the specimens (high stress level: 0.6). At low stress level (0.3) the loading was performed at 2 or 28 days' age. However, the stress/compressive strength ratio decreased in the concretes that were young when loaded, from 0.6 to 0.1 in some cases, due to the ongoing hydration of HPC. The concrete loaded at 28 days' age obtained the highest long-term stress/compressive strength ratio. Table 5 shows the methods, devices, age at loading, and stress level used to obtain the different parameters.

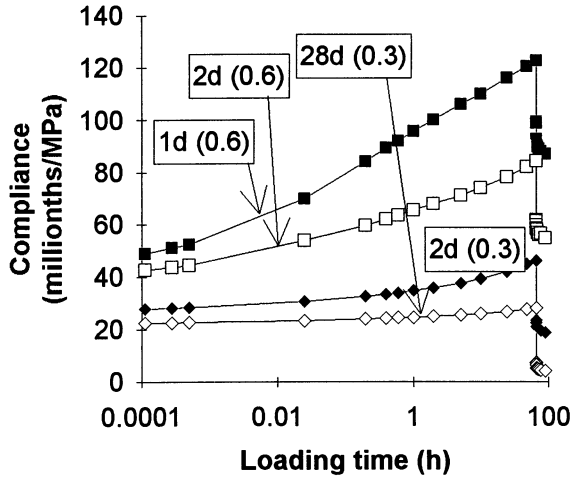

FIGURE 1. Short-term creep of HPC mix 6.

Results

Short-Term Basic Creep

The loading in the MTS machine was performed within about 0.01 seconds in an effort to separate elastic deformation from viscous elastic and plastic creep deformations [12]. The accuracy of the loading in the MTS machine was within ±0.1%. Figure 1 shows typical results of a short-term test, HPC mix 6. Appendices 1 through 8 show the results of creep compliance of short-term loading of all the concrete mixes [7]. The

TABLE 5. Experimental methods, devices, age at loading, and stress level [7]

Type of Experiment	Type of Device	Age at Start (days)	σ/f_c
Short-term creep	MTS	1 and 2	0.6
Short-term creep	MTS	3 and 28	0.3
Long-term creep	Spring loading	1 and 2	0.6
Long-term creep	Spring loading	3 and 28	0.3
Autogenous shrinkage	Mechanical	1, 2, 3 and 28	
Compressive strength	Hydraulic press	1, 2, 3, 5, 6, 7, 28, 360, and 1440	
Internal relative humidity	Dew-point meter	1, 2, 3, 5, 6, 7, 28, 360, and 1440	
Hydration	Oven and scale	1, 2, 3, 5, 6, 7, 28, 360, and 1440	

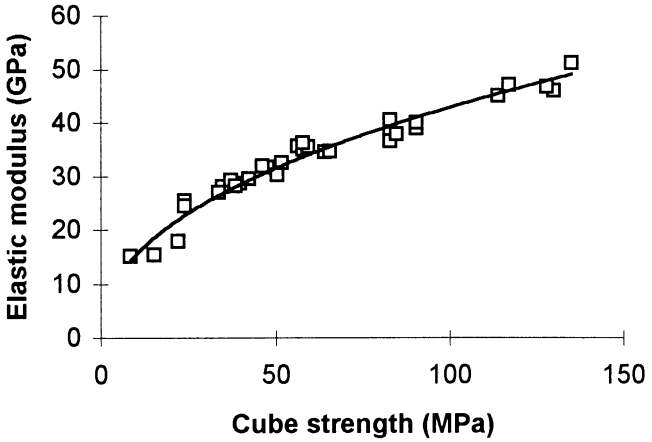

FIGURE 2. Elastic modulus (GPa) of HPC vs. cube compressive strength (MPa).

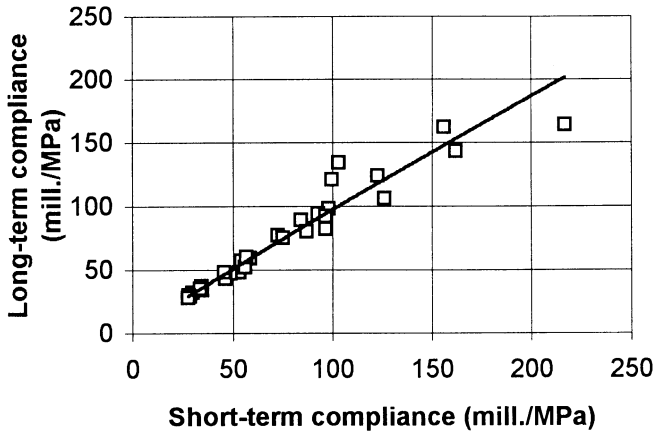

FIGURE 3. Long-term creep compliance vs. short-term creep compliance after 66 hours.

specimens were unloaded after 66 hours of loading. At a corresponding strength of mature HPCs (28 days) the elastic deformation, when the specimens were unloaded, coincided well with the deformation 0.01 seconds after loading (Figure 2). The elastic modulus of mature HPC was similar to the deformation modulus that occur in 0.01 seconds. The following relation was calculated for the strength and elastic modulus of sealed HPC:

$$E_{0.01s} = 5.4 \cdot (f_c)^{0.46} \quad \{10 < f_c < 160 \text{ MPa}\} \qquad (1)$$

where $E_{0.01s}$ denotes the elastic modulus 0.01 seconds after quasi-instantaneous loading (GPa); and f_c denotes the cube compressive strength when the cylinder was loaded (MPa).

Long-Term Deformations

The long-term loading was performed in traditional spring-loading devices. The loading of cylinders in the spring-loading devices was raised by about 1 MPa/s. A precision load cell was used to control the loading. The loading was maintained at a constant level at each occasion of measuring with the precision load cell (within ±0.1 kN). The accuracy of the loading between the time of measurement was ±5%. It was also important to compare the creep compliance of the short-term creep tests after 66 hours of loading and the creep compliance of the long-term creep tests after 66 hours of loading. Figure 3 shows the long-term creep compliance of all HPCs after 66 hours of loading vs. the short-term creep compliance after 66 hours of loading [7]. According to Figure 3 the creep compliance obtained after 66 hours in the spring-loading devices coincided well with the compliance obtained in the MTS machine. The way or rate of loading evidently did not have any influence on the measured creep compliance (Figure 3). Creep properties of the HPCs obtained by the quasi-instantaneous loading in the MTS-machine were thus also applicable to the long-term creep compliance studies. After 2 years of loading, cylinders made of HPC mixes 2, 3, 5, 6, and 8 (Table 3) were unloaded to obtain the long-term elastic modulus, the viscous elastic, and the plastic creep. (The results of viscous elastic and plastic creep are not presented in this article.) Figure 4 shows typical results of a long-term test, HPC mix 6. Appendices 9 through 16 show the long-term creep compliance measured in traditional spring-loading devices [7]. A portion of the basic creep is attributed to autogenous shrinkage, which occurred due to the self-desiccation of the concrete [13]. The self-desiccation in HPC caused substantial pore water depression in HPC [11], which in turn caused autogenous shrinkage. Figure 5 shows the autogenous shrinkage of the HPCs (results from 28 cylinders since 5 cylinders showed too large moisture losses). Figure 6 shows the self-desiccation of the HPCs. The self-desiccation was studied for 22 hours by use of dew-point meters on fragments of cubes used for stud-

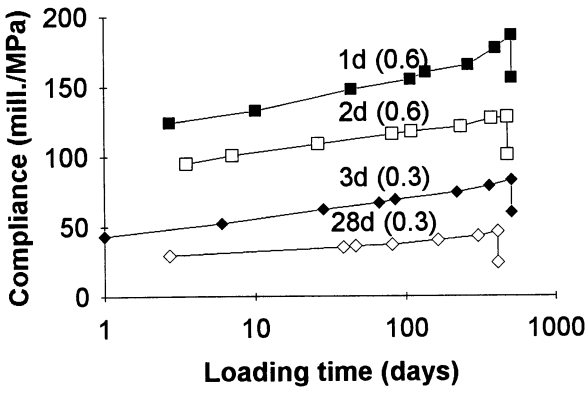

FIGURE 4. Long-term creep of HPC mix 6.

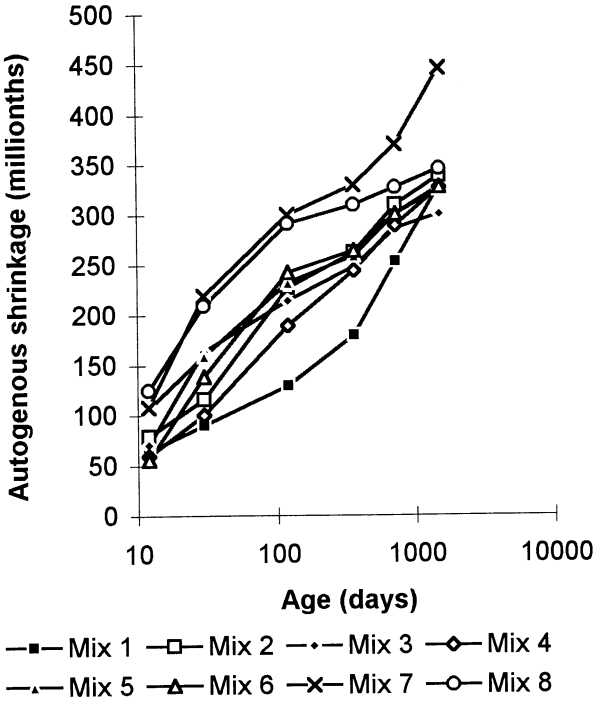

FIGURE 5. Autogenous shrinkage of different HPC mixes specified in Table 3.

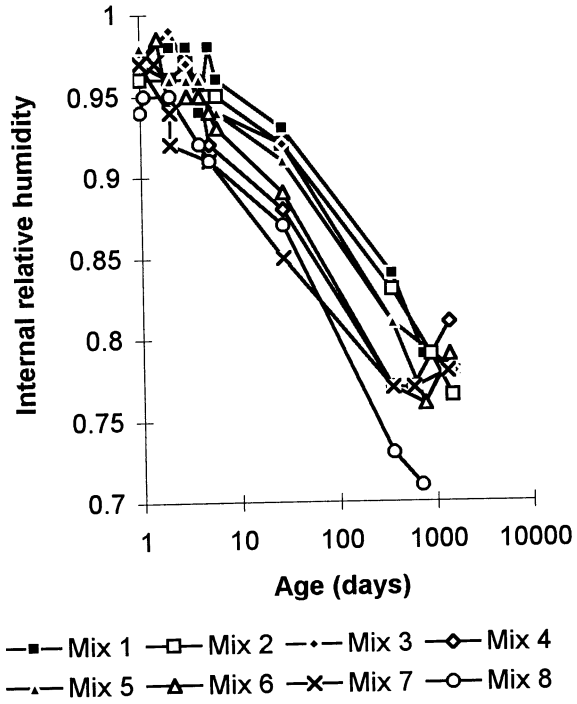

FIGURE 6. Self-desiccation of different HPC mixes specified in Table 3.

ies of compressive strength [13]. The dew-point meters were salt-calibrated according to ASTM E 104-85 (1985, Standard Practice for Maintaining Constant Relative Humidity by Means of Aqueous Solutions).

Basic Creep after Heat Curing

From a practical point of view, it was of interest to study the creep of HPC after heat curing. In large structures the temperature of HPC often rises 25°C during the early curing. In these experiments, studies at various temperatures after a period of heat curing only were performed with HPC mix 6 (Table 3). The tested HPC cylinder was built into a climate box within the MTS machine. The climate box was supplied by air conditioning from a climate room. The HPCs were heat cured at internal concrete temperatures shown in Figure 7. The temperature was measured with thermocouples that were cast into the HPC specimen. For the first 16 hours after casting the specimens were cured at about 45°C. During preparation with measurement transducers the temperature was lowered to about 20°C. The same loading and unloading procedure was used as in the short-term studies presented above. The loading on the HPC cylinders was performed at 1 day's age. The cylinders were unloaded after 66 hours of loading. Figure 8 shows compliance vs. loading time at various temperatures and stress levels.

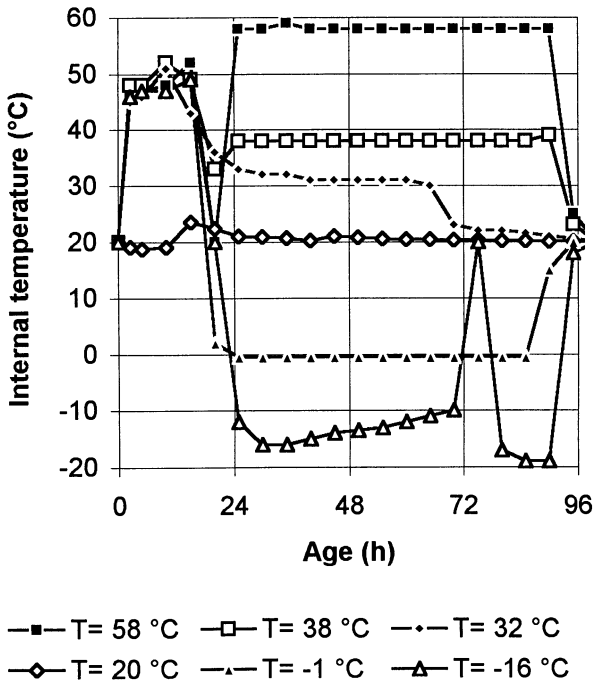

FIGURE 7. Temperatures at heat curing.

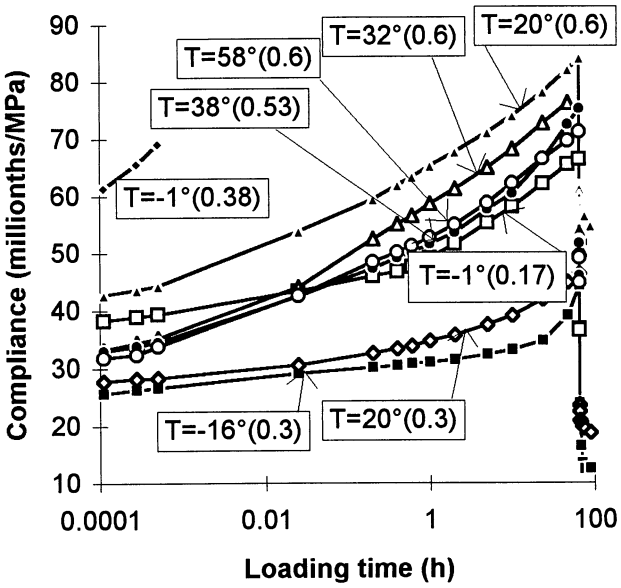

FIGURE 8. Short-term creep of HPC mix 6.

Analysis

Elastic Modulus and Porosity

It is well-known that there exists a relation between elastic modulus and porosity for NSC. However, for HPC the porosity is low, which may change the influence of porosity on the elastic modulus. It was then of interest to obtain this relation between elastic modulus and porosity for HPC. A composite model was used to calculate the elastic modulus of mature HPC [14]:

$$E_c^{\,n} = A \cdot E_a^{\,n} + (1 - A - B) \cdot E_p^{\,n} \qquad \{15 < E_c < 50 \text{ GPa}\} \tag{2}$$

where for n, $n = 1$ for a parallel model when $E_p \gg E_a$, and $n = -1$ for a serial model when $E_p \ll E_a$; A denotes the aggregate volume share given below; B denotes the volume share of chemical shrinkage and air-entraining given below; E_a denotes the elastic modulus of the aggregate (GPa); E_c denotes the elastic modulus of the concrete (GPa); and E_p denotes the elastic modulus of the cement paste (GPa).

$$A = w_a/\rho_a \tag{3}$$

$$B = (w - 0.19 \cdot \alpha \cdot c)/\rho_w - \mu_{ai} \tag{4}$$

where c denotes the cement content (kg/m^3); w denotes the mixing water (kg/m^3); w_a denotes the weight of aggregate (kg/m^3); α denotes the degree of hydration of the cement; μ_{ai} denotes the volume share of air-entraining; ρ_α denotes the density of the aggregate (kg/m^3); and ρ_w denotes the density of the water (kg/m^3).

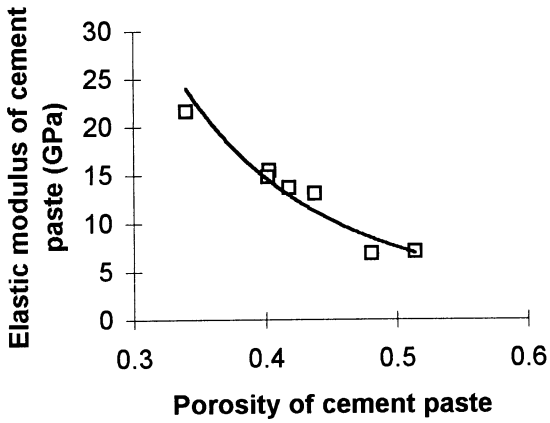

FIGURE 9. Elastic modulus of the cement paste after 0.01 seconds of loading vs. the porosity of the cement paste.

Equation 2 was used to calculate the elastic modulus of the cement paste at 28 days. The elastic modulus of HPC was known according to eq 1 and Figure 1. The degree of hydration (α) was obtained by ignition for 16 hours of all the samples of HPCs after the compressive strength tests were performed [7] and estimated according to a procedure previously reported [13,15]. The elastic modulus of aggregate was provided in Table 1 [6]. Further data required to use eqs 3 and 4 were provided in Table 3. The elastic modulus was calculated according to eq 2 with the exponent $n = -0.67$. The porosity of the cement paste was calculated according to the following equation:

$$P_p = \frac{w - 0.19 \cdot \alpha \cdot c + l}{\frac{c}{\rho_c} + w + l} \qquad \{0.35 < P_p < 0.55\} \tag{5}$$

where l denotes the air volume in the concrete (l/m^3) P_p denotes the porosity of the cement paste according to eq 5; and ρ_c denotes the density of the cement (kg/m^3). The air volume in the HPC was measured (cp. Table 3). The remaining symbols in eq 5 are given above. Figure 9 shows the elastic modulus of the cement paste versus the porosity of the cement paste. From Figure 9 an equation for the elastic modulus of cement paste 0.01 seconds after loading ($E_{p,0.01}$) was calculated (GPa):

$$E_{p,0.01} = 0.95 \cdot P_p^{\,-3.0} \qquad \{0.35 < P_p < 0.55\} \tag{6}$$

The elastic modulus of the cement paste also was related to the capillary porosity $\{(P_{cap})_p\}$:

$$(P_{cap})_p = \frac{w - 0.39 \cdot \alpha \cdot c + l}{\frac{c}{\rho_c} + w + l}$$

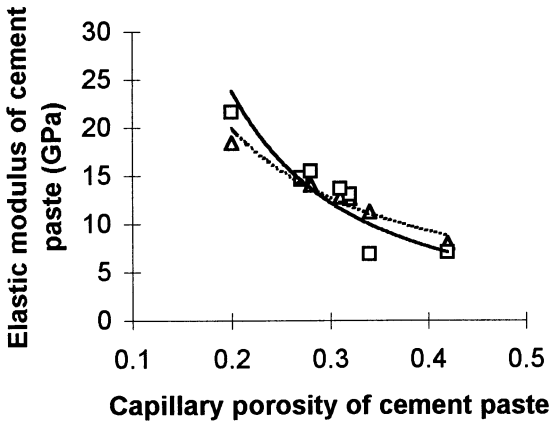

FIGURE 10. Elastic modulus of the cement paste at 0.01 seconds of loading vs. the capillary porosity of the paste [7,16].

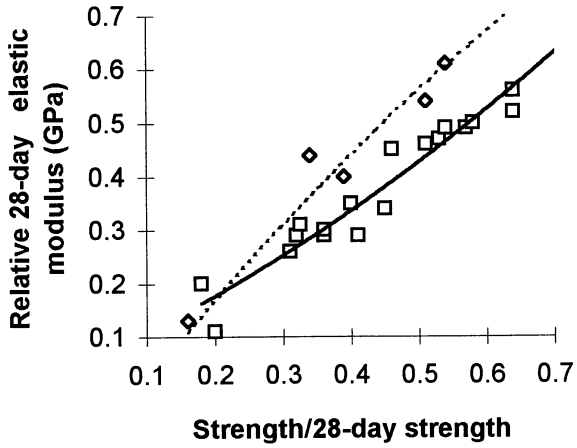

FIGURE 11. The 28-day relative elastic modulus of cement paste after 0.01 seconds of loading vs. the 28-day relative compressive strength. Dotted line = HPC with air-entraining.

$$\{0.20 < (P_{cap})_p < 0.45\} \tag{7}$$

The remaining symbols used in eqs 6 and 7 are given above. Figure 10 shows the elastic modulus of the mature cement paste vs. the capillary porosity of the paste the 0.01 seconds after loading. In Figure 10 there are two regression lines indicated. The solid line in Figure 10 indicates the elastic modulus estimated according to eq 2 with $n = -0.67$. The dotted line in Figure 10 indicates an expression estimated according to [16] (GPa):

$$E_{p,0.01} = 1.71 \cdot (P_{cap})_p^{-1.64} \qquad \{0.20 < (P_{cap})_p < 0.45\} \tag{8}$$

$$E_p = 32 \cdot (1 - (P_{cap})_p)^{2.5} \qquad \{0.20 < (P_{cap})_p < 0.45\} \tag{9}$$

The values of the elastic modulus calculated using eqs 8 and 9 agreed reasonably well. The elastic modulus was similar in HPC and NSC cement paste at constant capillary porosity. The influence of the porosity was greater in HPC than in normal cement paste.

It also was interesting to compare early development of elastic modulus of cement paste at varying maturity. Figure 11 shows the 28-day relative elastic modulus of the cement paste after 0.01 seconds of loading vs. the 28-day relative compressive strength. The elastic modulus was calculated according to eq 2 with the exponent, $n = -0.674$. The elastic modulus in cement paste was larger in HPC with air-entraining than in HPC without air-entraining when the maturity was held constant. The moisture movement in the cement paste probably explained this. When air-entraining existed, the moisture probably moved more rapidly into the air-filled space at loading than if no air-entrainment existed. This caused a larger increase of the elastic modulus than in a paste without air-entraining. From Figure 11 the following equation of the early development of the elastic modulus in the cement paste was calculated (see eq 10):

$$E_p/E_{p28} = A \cdot (f_c/f_{c28})^2 + B \cdot (f_c/f_{c28}) + C \qquad \{8 < E_p, E_{p28} < 22\ GPa\} \tag{10}$$

where E_p denotes the elastic modulus of the cement paste 0.01 seconds after loading (GPa); E_{p28} denotes the 28-day elastic modulus of the paste 0.01 seconds after loading (GPa); A, B, C denote constants given in Table 6; f_c denotes the compressive strength of the concrete (MPa); and f_{c28} denotes the 28-day compressive strength of the concrete (MPa).

Short-Term Basic Creep

From a practical point of view it is of great interest to estimate the early deformation of HPC at early ages. The compliance during the 66 hours of short-term loading was separated into an elastic part and another creep component due to the loading [12]. The elastic part was estimated by eq 1. The compliance creep curves shown in Appendices 1 through 8 were analyzed according to a logarithmic function [7]. The slope of these curves expressed the early creep rate [12] of the HPCs. It was appropriate to separate the creep rate of

TABLE 6. Constants A, B, and C in eq 10.

Constant	A	B	C
Air-entraining agent	−0.542	1.695	−0.147
No air-entraining	0.369	0.577	0.046

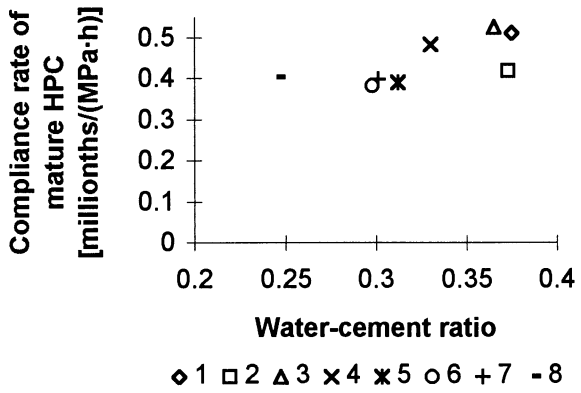

FIGURE 12. Compliance rates of mature HPC during 66-hour short-term tests vs. the water-cement ratio. The type of HPC is indicated (Table 3).

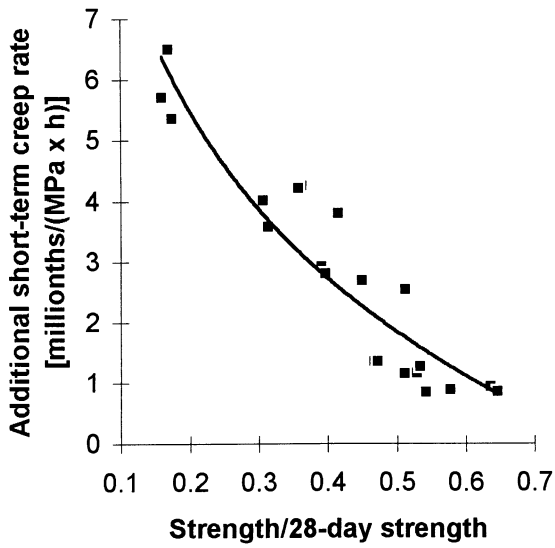

FIGURE 13. Additional creep rate at early ages vs. the ratio of the compressive strength at loading and the 28-day compressive strength at loading and th 28-day compressive strength, f_c/f_{c28}.

young HPC from that of mature HPC. Figures 10 shows the creep rate of mature HPC. Figure 12 shows that mature HPCs with 5% silica fume (mixes 1 and 4) or/and air-entraining (mixes 1 and 3) exhibited a larger creep rate than HPCs with 10% silica fume. The reason is attributed to the decrease of porosity that occurred when more silica fume was used in the HPC or alternatively the increased porosity of the paste caused by the air-entraining; compare the analysis of the elastic modulus above. From Figure 12 it also was concluded that the creep compliance rate was independent of the type of aggregate. The short-term creep rate for the HPCs with 5% silica fume or/and air-entraining was ≈0.5 millionths/(MPa · h) and ≈0.4 millionths/(MPa · h) for the remaining HPCs independent of w/c. This result was astonishing since a lower creep rate was expected at lower w/c. Figure 13 shows the additional creep rate of young HPC. Figure 13 shows a substantial increase of compliance creep rate for compressive strength to 28-day compressive strength ratio at loading less than 60% ($f_c/f_{c28} < 0.6$). The following equation was obtained for the short-term deformations at early ages [7]:

$$J_{ee}(t, t', f_c/f_{c28}) = [k_i \cdot 0.4 - 3.98 \cdot ln(f_c/f_{c28})] \times \int d(t - t')/(t - t') + 1000/E_{t'} \quad \{0.15 < f_c/f_{c28} < 1\} \tag{11}$$

where $J_{ee}(t, t', f_c/f_{c28})$ denotes the creep compliance of young HPC (millionths/MPa); f_c/f_{c28} denotes the compressive strength to the 28-day strength ratio at loading; $k_i = 1.25$ for HPCs with 5% silica fume or/and air-entraining or $k_i = 1$ otherwise; t denotes the age of the concrete (hours); $\{0.0001 < (t - t') < 66$ hours$\}$; $E_{t'}$ denotes the elastic modulus when loading the concrete (GPa).

Equation 11 is plotted in Figure 13. For the early creep compliance of mature HPC, $J_{em}(t, t', f_c/f_{c28} = 1)$, the following equation was obtained (millionths/MPa; symbols given above):

$$J_{em}(t, t) = k_i \cdot 0.4 \cdot \int d(t - t')/(t - t') + 1000/E_{t'} \quad \{f_c/f_{c28} = 1\} \tag{12}$$

Autogenous Shrinkage

The long-term deformations of HPC also consisted of autogenous shrinkage. The autogenous shrinkage was studied on 33 cylinders for 2 years (Figure 5). However, 5 of the cylinders obtained moisture losses larger than 4 g over 2 years (estimated on a specimen weight of 1.8 kg) and were not used in the average values shown in Figure 5. Figure 6 shows that the moisture stability was maintained in the specimens since the internal relative humidity (Ø) in the HPC did not fall below 0.70 [10]. Ø may be estimated according to Figure 6 or reference [17]. Both type and amount of silica fume had an influence on the autogenous shrinkage. Probably the specific surface of silica fume affected the amount of shrinkage (cp. Table 1). The following equations were calculated for the autogenous shrinkage of HPC [7] (mm/m):

$$\varepsilon_{bg} = k_5 \cdot 0.17 \cdot [3.2 + ln(1 - Ø)]$$

$$\{0.75 < Ø < 0.95\} \quad (13)$$

$$\varepsilon_{bs} = k_5 \cdot 0.35 \cdot [2.5 + ln(1 - Ø)]$$

$$\{0.70 < Ø < 0.90\} \quad (14)$$

where $k_5 = 0.8$ for 5% silica fume, or $k_5 = 1$ for 10% silica fume; ε_{bg} denotes autogenous shrinkage with 5–10% granulated silica fume (mm/m); ε_{bs} denotes the autogenous shrinkage with 5–10% silica fume slurry (mm/m); and Ø denotes internal relative humidity after self-desiccation according to reference [7].

Equations 13 and 14 were confirmed by other results [18]. The self-desiccation of HPC with 5–10% granulated silica fume was estimated according to [19]:

$$Ø(wbr_{eff}, t) = 0.38 \cdot (wbr_{eff} + 2.4 - 0.1 \cdot ln\ t) + Ø_{sl} \quad (15)$$

$$wbr_{eff} = w/(c + 2 \cdot s) \quad (16)$$

where c denotes the cement content in the concrete (kg/m^3); s denotes the content of silica fume in the concrete (kg/m^3); t denotes the age of the concrete {1 < t < 1000 days}; w denotes the mixing water content in the concrete (kg/m^3); and $Ø_{sl}$ denotes a correction for 5–10% silica fume slurry, $Ø_{sl} = -0.035$, at age ≤28 days (see eqs 15 and 16).

Long-Term Deformations

The quasi-instantaneous and short-term deformations (until 2.7 days) were described by eqs 11 and 12. In order to describe the long-term basic creep, a parameter study was realized. The purpose of this study was to define principal parameters affecting the creep properties such as the aggregate content, the cement content, and the influences of compressive strength and water content. Figure 14 shows the principal parameters of the HPCs vs. the long-term creep rate of mature HPC. The effect of compressive strength was found to be the principal parameter of the long-term creep properties. Figure 15 shows the long-term creep rate of mature HPC vs. compressive strength. Figure 16 shows the additional creep rate in HPC at early ages. To obtain a relationship for the long-term creep, an adjustment was made in relation to the content of silica fume when the HPC was loaded in a mature state:

$$J_l(t, t', f_c/f_{c28}) = [k_5 \cdot 0.018 \cdot (300 - f_{c28}) - k_{ais} \cdot 4.4 \cdot ln(f_c/f_{c28})] \times \int d(t - t')/(t - t') \quad \{2.7 < (t - t') < 1000 \text{ days}\} \quad (17)$$

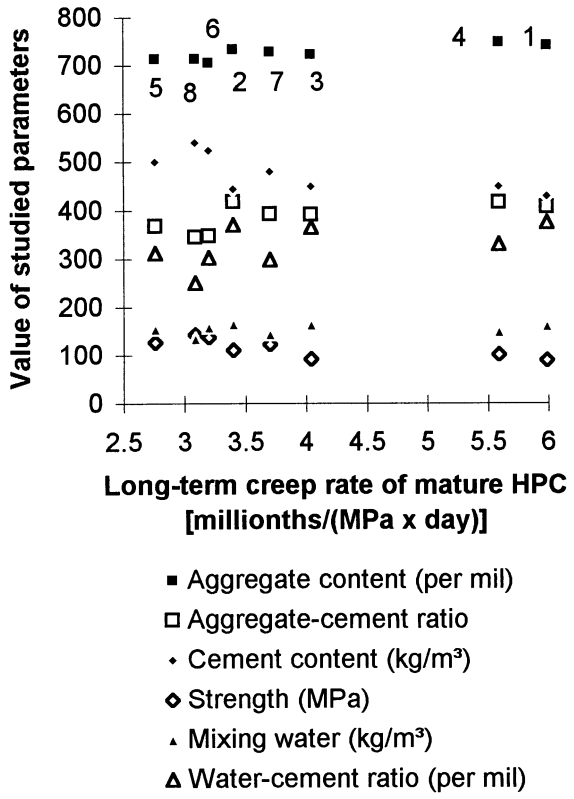

FIGURE 14. Parameters influencing the long-term creep rate of HPC. Type of HPC is given.

where $k_{ais} = 1.3$ for HPC with 5% air-entraining, $k_{ais} = 0.7$ for HPC with silica fume slurry; or $k_{ais} = 1$ otherwise; $k_5 = 1.5$ for HPC with 5% silica fume, or $k_s = 1$ for HPC with 10% silica fume; and $J_l(t, t', f_c/f_{c28})$ denotes the long-term compliance in HPC after 2.7 days' age (millionths/MPa).

The remaining symbols in eq 17 are given above. Compliance at 2.7 days (calculated by eqs 11 or 12 above) to be deduced from eq 17. In order to estimate

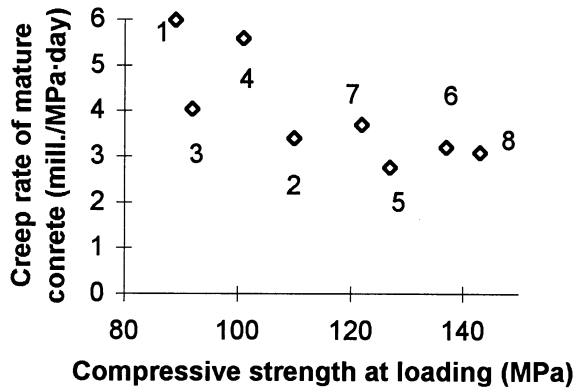

FIGURE 15. Creep rate of mature HPC vs. compressive strength [millionths/(MPa · day)].

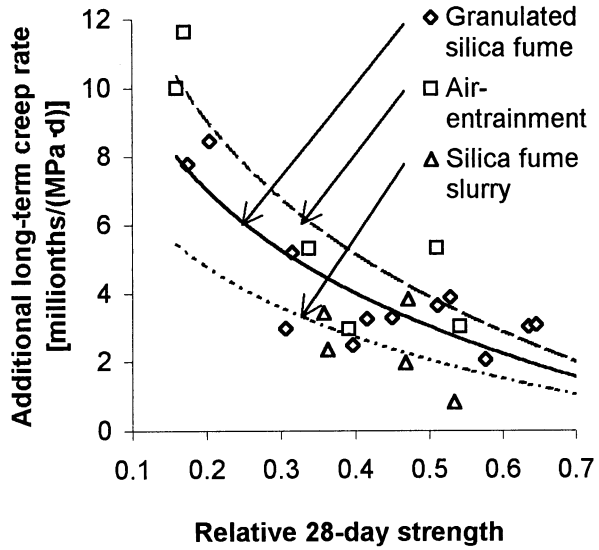

FIGURE 16. Additional creep rate at early ages [millionths/(MPa · day)].

the total deformation, the following procedure was used (definitions are given in the list of symbols in Appendix 17):

$$\varepsilon = J \cdot \sigma = \sigma[J_{ee}(t, t', f_c/f_{c28}) + J_l(t, t', f_c/f_{c28})] \quad \{0.15 < f_c/f_{c28} < 1\} \tag{18}$$

$J_{ee}(t, t', f_c/f_{c28}) + J_l(t, t', f_c/f_{c28})$ are given by eqs 11, 12, and 17. Equations 17 and 18 coincided well with field experiments on 27 HPC beams [19].

Creep after Heat Curing

Analyses were carried out related to both temperature and stress level. At −1°C rapid failures of the specimens were observed both at $\sigma/f_c = 0.6$ and at $\sigma/f_c = 0.38$. At −1°C the short-term tests only were carried out at a stress to compressive strength ratio, $\sigma/f_c = 0.17$. Remaining tests at temperatures other than −1°C were carried out at $\sigma/f_c = 0.3$ (−16°C) or at $\sigma/f_c \approx 0.6$ (32°, 38°, and 58°C). Creep results of HPC type 6 cured at 20°C loaded at 2 days are shown in Figure 8. The failures of the specimens at −1°C was probably due to formation of salts only stable at this temperature [20–22]. (At −1°C no freezeable water exists in HPC owing to self-desiccation.) Figure 17 shows the creep rate vs. the stress to compressive strength ratio at loading. The creep rate vs. the temperature of the specimen is shown in Figure 18. The creep rate of HPC at −1°C was substantially larger than at other temperatures. The following equations of the creep rate were calculated based on Figures 17 and 18:

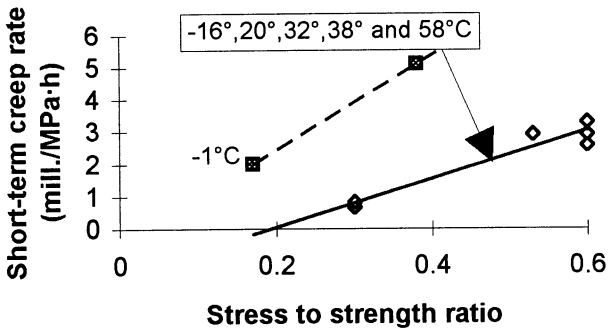

FIGURE 17. Creep rate of heated HPC vs. the stress to compressive strength ratio at loading.

$$dJ_{-1^\circ}/dt = [16/(t - t')] \cdot (\sigma/f_c)^{1.16} \quad \{0.17 < (\sigma/f_c) < 0.38\} \tag{19}$$

$$dJ/dt = [8.8/(t - t')] \cdot (\sigma/f_c)^2 \quad \{0.30 < (\sigma/f_c) < 0.60\} \tag{20}$$

$$dJ/dt = [0.036/(t - t')] \cdot (T + 36) \quad \{-20 < T < 60°C\} \tag{21}$$

where f_c denotes the compressive strength when loading the concrete (MPa); dJ_{-1°/dt denotes the creep rate of HPC at −1°C (millionths/MPa · hour); dJ/dt denotes the creep rate at −16°, 20°, 32°, 38°, and 58°C (millionths/MPa · hour); T denotes the temperature of the HPC {−20 < T < 60°C}; and σ denotes the stress in the concrete during the creep tests (MPa) (see eqs 19, 20, and 21).

Comparison with Previous Research

Creep Compliance

Figure 19 shows the initial and the creep compliance vs. the compressive cylinder compressive strength of mature HPC [23]. The initial compliance occurs after the

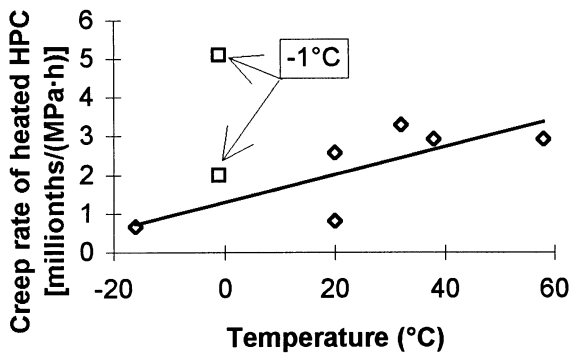

FIGURE 18. Creep rate vs. the temperature of the specimen.

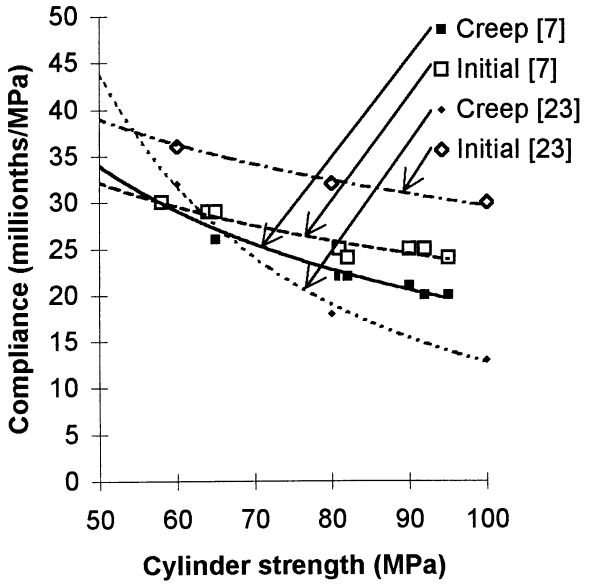

FIGURE 19. Compliance vs. compressive cylinder strength of mature concrete [7,23].

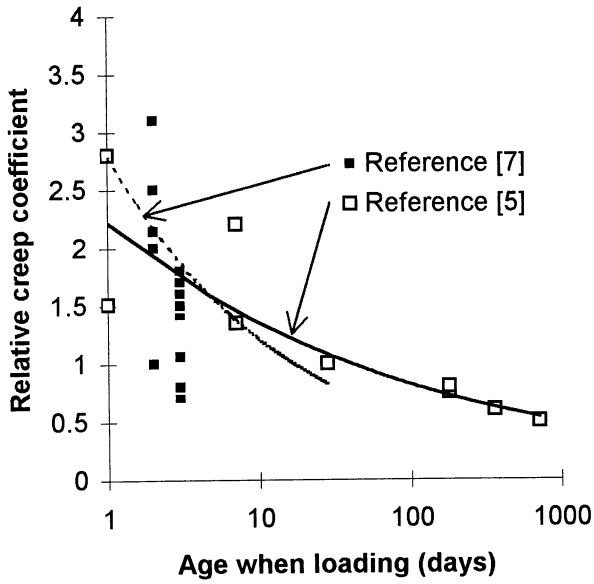

FIGURE 20. Results of creep of young concrete [5,7].

elastic deformation followed by the creep deformation. From Figure 19 the following equation was calculated for the compliance:

$$J_{in} = 220 \cdot (f_c')^{-0.5} \tag{22}$$

$$J_{cr} = 80000 \cdot (f_c')^{-2} \tag{23}$$

where f_c' denotes the cylinder compressive strength of the concrete (MPa); J_{cr} denotes the compliance after reduction of the elasticity (millionths/MPa); and J_{in} denotes the initial compliance after the elastic deformation (millionths/MPa).

According to Figure 19 the total compliance of mature concrete (with the initial compliance estimated after 100 seconds of loading) [7] coincided reasonably well with results according to reference [23]. However, the creep compliance was slightly larger according to reference [7] than according to reference [23]. Figure 20 shows results of creep of young HPC [5], which coincided well with reference [7].

In order to compare previous research with the present study calculations were performed with eqs 11, 17, 22, and 23. However, the type and amount of silica fume in HPC of reference [23] was not known. The calculations were performed for 5% and for 10% granulated silica fume. The cylinder compressive strength (f_c') was calculated on the cube compressive strength (f_c) using the following relation [11]:

$$f_c' = 0.71 \cdot f_c \tag{24}$$

where f_c denotes the compressive strength of a 100-mm cube (MPa); and f_c' denotes the compressive strength of a cylinder 55 mm in diameter (MPa).

The calculated compliance of the present study coincided reasonably well with previous research, also taking into account that the exact HPC mix of reference [23] was unknown (Figures 19 and 20) [5,7,23]. The initial compliance calculated according to the previous study was [23] more affected by the compressive strength than were the results of the present study [7].

Elastic Strain

In this study only sealed specimens of HPC were studied. Due to the high moisture content in sealed HPC specimens the elastic modulus will be larger than in dried HPC specimens [23]. The elastic modulus of sealed HPC according to eq 1 thus is larger than the elastic modulus of HPC according to the following equation [19] (eq 25 was evaluated from a relationship with cylinder compressive strength by use of eq 24):

$$E = 11 \cdot (f_c)^{0.3} \tag{25}$$

where E denotes the elastic modulus (GPa); and f_c denotes the cube compressive strength (MPa).

Summary and Conclusions

The following conclusions for HPC conform to established facts for NSC:

- Elastic modulus is related to compressive strength and porosity as demonstrated in NSC.
- The creep rate was dependent on both the duration of loading and the maturity of the HPC.
- Creep properties of the HPCs obtained by the quasi-instantaneous loading were applicable to the long-term creep compliance studies performed with a much lower loading rate.
- Specific creep was shown to be reduced with increase in silica fume content.
- Autogenous shrinkage was reduced by the use of granulated silica fume instead of silica fume slurry, probably owing to the larger fineness of the silica fume slurry.

The modulus of elasticity of HPC has a strong correlation to the compressive strength when loading the HPC. The value of elastic modulus was confirmed related to the compressive strength when the HPC specimens were unloaded. The elastic modulus was also related to the porosity of the cement paste of the HPC by parallel studies carried out on sealed cubes. The creep compliance of HPC at early ages was dependent not only on the loading time of the HPC but also on the maturity when loading. The creep rate was slightly reduced when 10% silica fume was used in the HPC as compared to 5% silica fume. However, the short-term studies indicated that the creep rate of mature HPC was fairly independent of the compressive strength, which may be an effect of the autogenous shrinkage of an HPC at lower w/c. The short-term basic creep rate of HPC after heat curing was observed to be twice as large at −1°C as at other temperatures (−16°, 20°, 32°, 38°, and 58°C), which is not previously seen in NSC. At −1°C, rapid failures of the specimens were observed at a stress to compressive strength ratio of both 0.6 and 0.38. At −1°C it was only possible to carry out the tests at a stress to compressive strength ratio as low as 0.17. Besides loading time, the long-term compliance of HPC was mainly dependent on the maturity and the compressive strength both when loading the HPC and at 28 days' age. Also in this case the creep was slightly reduced by use of 10% silica instead of 5%. The calculated long-term compliance of the present study coincided reasonably well with previous research, taking into account that the exact HPC mix was unknown. However, the observed creep compliance was slightly larger than previously seen. The initial compliance calculated according to the previous studies was more affected by the strength than were the results of the present study. The autogenous shrinkage was mainly dependent on the internal relative humidity in HPC, which was detected by

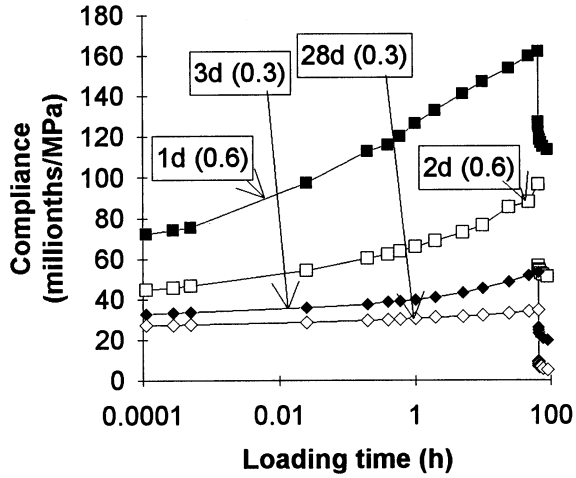

APPENDIX 1. Short-term creep, HPC mix 1.

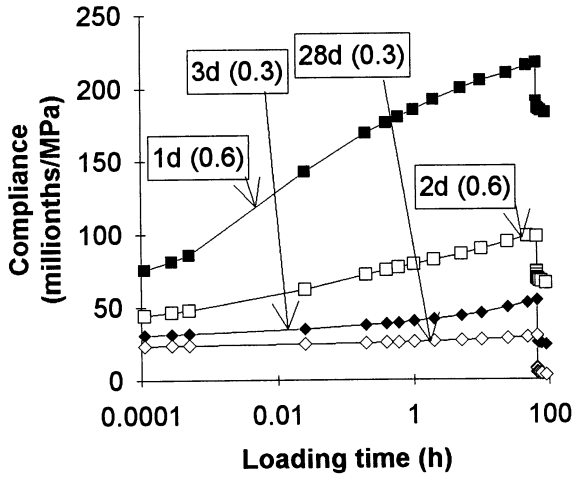

APPENDIX 2. Short-term creep, HPC mix 2.

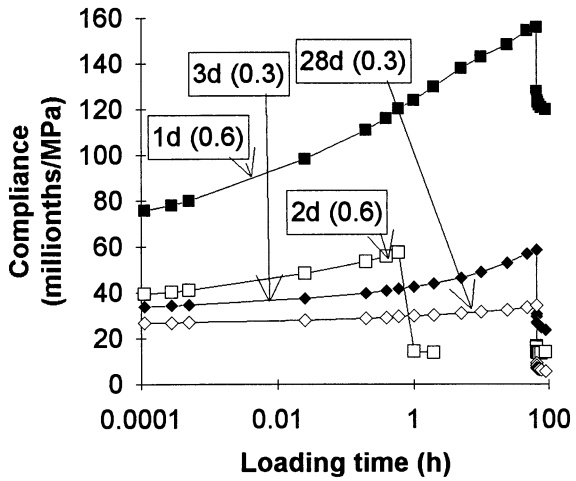

APPENDIX 3. Short-term creep, HPC mix 3.

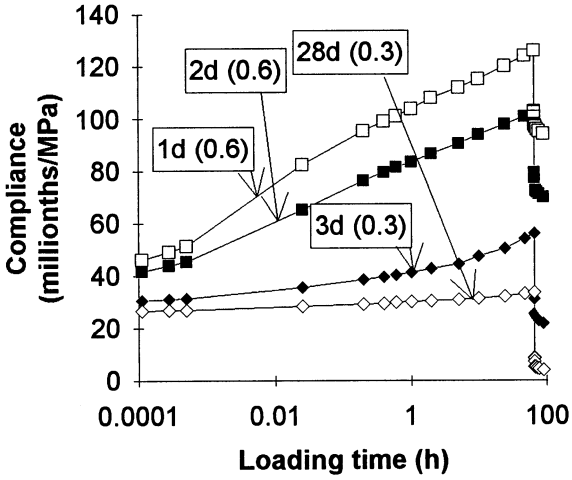

APPENDIX 4. Short-term creep, HPC mix 4.

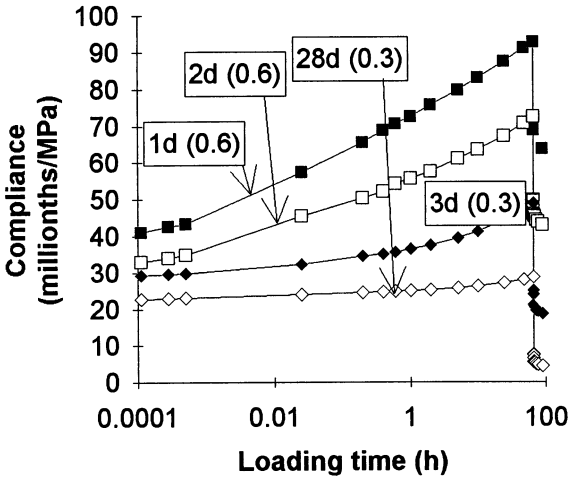

APPENDIX 5. Short-term creep, HPC mix 5.

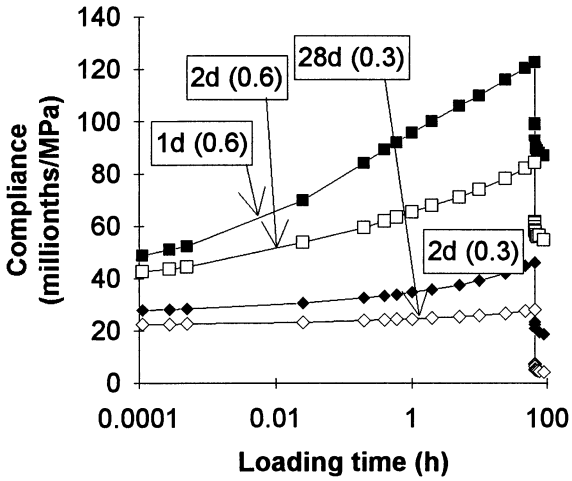

APPENDIX 6. Short-term creep, HPC mix 6.

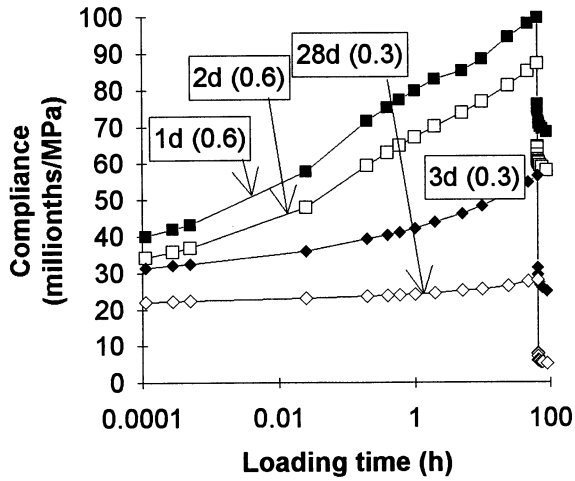

APPENDIX 7. Short-term creep, HPC mix 7.

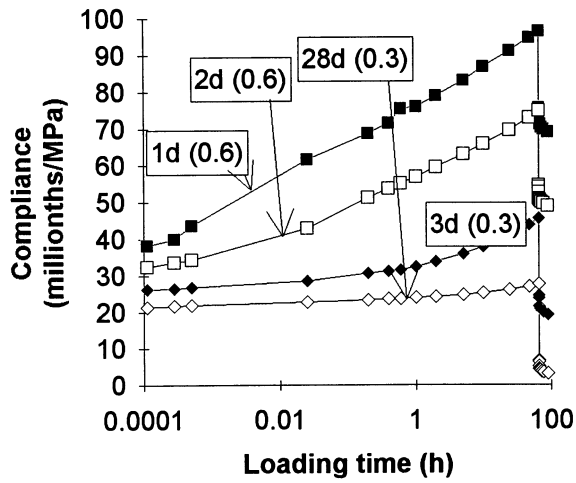

APPENDIX 8. Short-term creep, HPC mix 8.

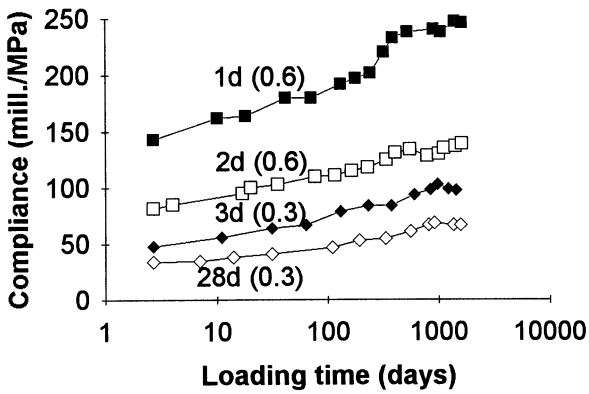

APPENDIX 9. Long-term creep, HPC mix 1.

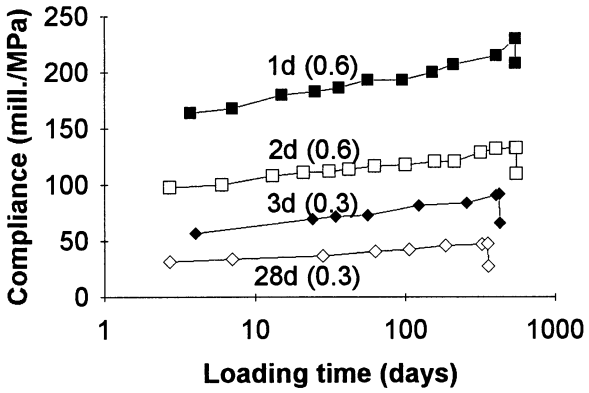

APPENDIX 10. Long-term creep, HPC mix 2.

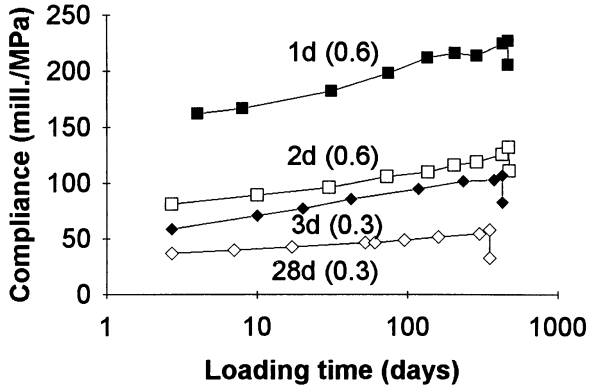

APPENDIX 11. Long-term creep, HPC mix 3.

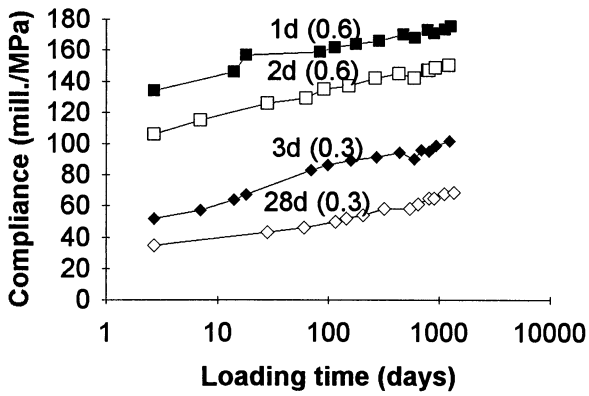

APPENDIX 12. Long-term creep, HPC mix 4.

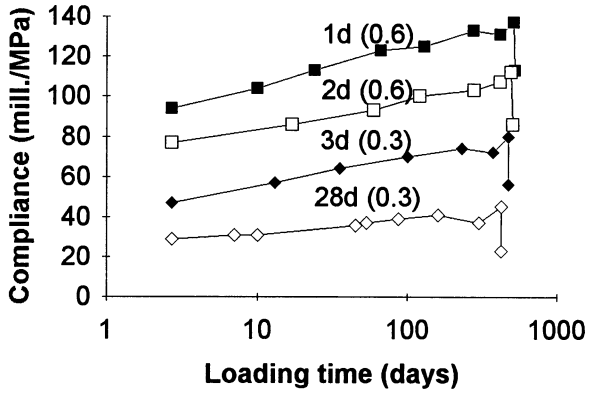

APPENDIX 13. Long-term creep, HPC mix 5.

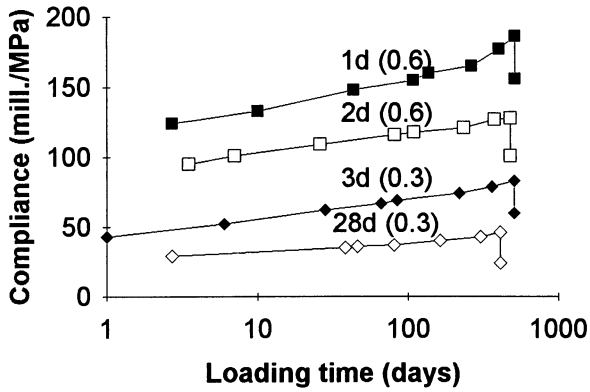

APPENDIX 14. Long-term creep, HPC mix 6.

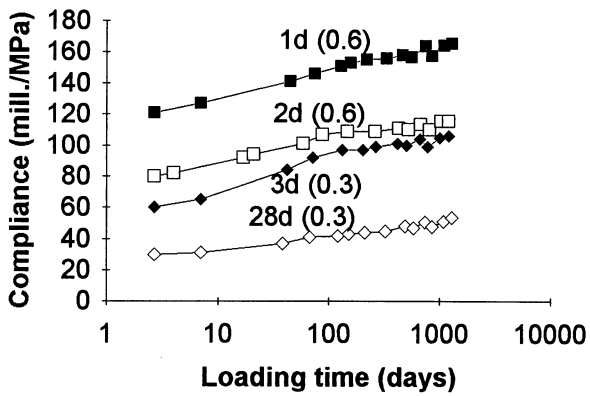

APPENDIX 15. Long-term creep, HPC mix 7.

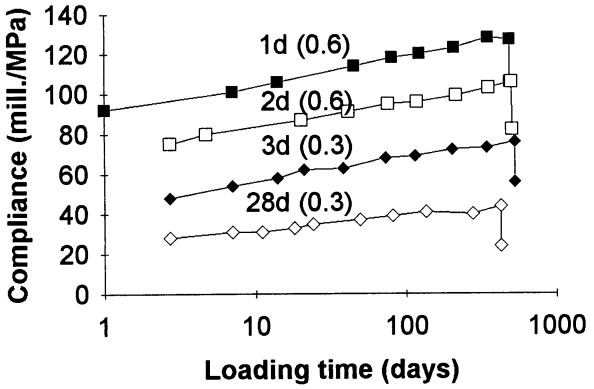

APPENDIX 16. Long-term creep, HPC mix 8.

parallel studies on sealed cubes. The autogenous shrinkage continued even after 2 years.

Appendix 17

List of symbols

a	aggregate content (kg/m^3)
c	cement content (kg/m^3)
d	days
f_c	compressive strength of 100-mm cube (MPa)
f'_c	compressive strength of cylinder 55 mm in diameter (MPa)
f_{c28}	28-day compressive strength of the concrete (MPa) hours
h	hours
k	specific volume of chemically bound water
l	air volume in the concrete (l/m^3)
mill.	millionths
s	seconds
t	age of the concrete (seconds, hours, or days)
t'	age when loading the concrete (seconds, hours, or days)
w/c	water/cement ratio (−)
w	amount of mixing water (kg/m^3)
w_a	weight of aggregate (kg/m^3)
w_n	weight of chemically bound water (kg/m^3)
A	aggregate volume share
B	volume share of chemical shrinkage and air-entraining
E	elastic modulus (GPa)
E_a	elastic modulus of the aggregate (GPa)
E_c	elastic modulus of the concrete (GPa)
E_p	elastic modulus of the cement paste (GPa)
J	compliance of the concrete, specific creep (ε/σ) (millionths/MPa)
$dJ_{-1°}/dt$	creep rate of HPC at −1°C (millionths/MPa · hour)
dJ/dt	creep rate at −16°, 20°, 32°, 38° and 58°C (millionths/MPa · h)
P_p	porosity of the cement paste according to eq 5
$(P_{cap})_p$	capillary porosity of the cement paste
T	temperature (°C)
α	degree of hydration of concrete (−)
ε	deformation of the concrete (compressive strain, −)
σ	compressive stress of concrete (MPa)
μ_{ai}	volume share of air-entraining
σ_α	density of the aggregate (kg/m^3)
ρ_c	density of the cement (kg/m^3)
ρ_w	density of the water (kg/m^3)
$Ø$	internal relative humidity of concrete (−)
(. . .)	stress to cube compressive strength ratio at loading (in Appendices)

Acknowledgments

Financial support from the Norwegian-Swedish Consortium for Research of High-Performance Concrete is hereby gratefully acknowledged. I am also most grateful to Professor Göran Fagerlund for his critical reviews.

References

1. Persson, B. In *Proceedings of the 16th Nordic Concrete Research Meeting: Espoo, Finland*; Norsk Betongforening, Norway, 1996; pp 85–87.
2. Helland, S. In *Proceedings of the 4th International Symposium on Utilization of High-strength/High-performance concrete*; Paris, 1996; pp 67–73.
3. Persson, B. In *Proceedings of the 3rd International Symposium on Utilization of High-strength/High-performance concrete*; Lillehammer, Norway, 1993; pp 882–889.
4. Penttala, V. In *Proceedings of the 16th Nordic Concrete Research Meeting: Espoo, Finland*; Norsk Betongforening, Norway, 1996; pp 70–71.
5. Müller, H.S. In *Proceedings of the Fourth Weimar Workshop on HPC*; Hochschule für Architektur und Bauwesen (HAB); Weimar, Germany, 1995; pp 145–162.
6. Hassanzadeh M. *Fracture Mechanical Properties of High-Performance Concrete, Report M4:05*; Division of Building Materials, Lund Institute of Technology: Lund, Sweden, 1994.
7. Persson, B. *Basic Creep of High-Performance Concrete, Report M6:14*; Division of Building Materials, Lund Institute of Technology: Lund, Sweden, 1995.
8. Acker, P. In *Proceedings of the Fifth International RILEM Symposium, Barcelona, Spain*; E&FN Spon, London, 1993; pp 849–858.
9. Schneider, U. Personal Communication; 1995.
10. Persson, B. *Mater. Struct.* **1997,** *30*, 293–305.
11. Persson, B. In *Proceedings of the 4th International Symposium on Utilization of High-strength/High-performance Concrete*; Paris, 1996; pp 405–414.
12. Bazant, Z.P. *Mater. Struct.* **1995,** *28*, 357–365.
13. Persson, B. *Adv. Cem. Based Mater.* **1996,** *3*, 107–123.

14. Hansen, T.C. *Theories of Multiphase Material Applied to Concrete, Cement Mortar and Cement Paste: Report 39*; The Swedish Cement and Concrete Research Institute, CBI: Stockholm, Sweden, 1966.
15. Byfors, J. *Plain Concrete at Early Ages: Report FO 3:80*; The Swedish Cement- and Concrete Research Institute, CBI: Stockholm, Sweden, 1980.
16. Fagerlund, G. *Relationship Between the Porosity and Mechanical Properties of Materials, Report 26*; Division of Building Physics, Lund Institute of Technology: Lund, Sweden, 1972, pp 197–221.
17. Persson, B. *Mater. Struct.* **1997,** *30*, 533–544.
18. Baroghel-Bouny, V. In *Proceedings of International Research Seminar on Self-desiccation and Its Importance in Concrete Technology*, Report TVBM-3075; Division of Building Materials, Lund Institute of Technology: Lund, Sweden, 1997.
19. Persson, B. *Creep of High Performance Concrete, Report M06:28*; Division of Building Materials, Lund Institute of Technology: Lund, Sweden, 1997.
20. Stark, J. Personal Communication, 1995 and 1997.
21. Stark, J.; Bollmann, K. *Untersuchungen zur Bildung von Oberflächenrissen in Betonfahrbahndecken*; Hochschule für Architektur und Bauwesen, HAB: Weimar, Germany, 1995.
22. Stark, J. Hochschule für Architektur und Bauwesen Weimar. Festkolloquium am 31. Mai 1996, Universität - Labor für Bau - und Werkstoffchemie: Siegen, Germany, 1996.
23. Bjerkeli, L.; Tomaszewics, A.; Jensen, J.J. In *2nd International Symposium on Applications of High Strength Concrete*; Berkeley, 1990.
24. Jaccoud, P.; Leclercq, A. In *Proceedings of the Fourth Weimar Workshop on HPC*; Hochschule für Architektur und Bauwesen (HAB); Weimar, Germany, 1995; pp 341–357.